Local Emergence of Peregrine Solitons: Experiments and Theory

Alexey Tikan[1], Stéphane Randoux[2], Gennady El[3], Alexander Tovbis[4], Francois Copie[2] and Pierre Suret[2]*

[1]Institute of Physics, Swiss Federal Institute of Technology Lausanne (EPFL), Lausanne, Switzerland, [2]University of Lille, CNRS, UMR 8523-PhLAM-Physique des Lasers Atomes et Molécules, Lille, France, [3]Department of Mathematics, Physics and Electrical Engineering, Northumbria University, Newcastle Upon Tyne, United Kingdom, [4]Department of Mathematics, University of Central Florida, Orlando, FL, United States

It has been shown analytically that Peregrine solitons emerge locally from a universal mechanism in the so-called semiclassical limit of the one-dimensional focusing nonlinear Schrödinger equation. Experimentally, this limit corresponds to the strongly nonlinear regime where the dispersion is much weaker than nonlinearity at initial time. We review here evidences of this phenomenon obtained on different experimental platforms. In particular, the spontaneous emergence of coherent structures exhibiting locally the Peregrine soliton behavior has been demonstrated in optical fiber experiments involving either single pulse or partially coherent waves. We also review theoretical and numerical results showing the link between this phenomenon and the emergence of heavy-tailed statistics (rogue waves).

1 INTRODUCTION

Recent mathematical works have recently triggered new research by unifying two old concepts, namely, the Peregrine soliton (PS) and the pulse compression in focusing nonlinear media [1]. The latter has been in particular widely investigated in optical fiber experiments for obvious application purposes [2], while the former has been extensively studied as a remarkable localized solution of the one-dimensional focusing nonlinear Schrödinger equation (1-D NLSE) [3]

$$i\psi_z + \frac{1}{2}\psi_{tt} + |\psi|^2\psi = 0, \tag{1}$$

for a complex wave field $\psi(t, z)$.

The universal NLSE (**1**) describes at leading order nonlinear waves in various physical systems and is integrable [4]. Its exact solutions called solitons on finite background (SFBs) such as Akhmediev breathers, Kuznetsov–Ma, and Peregrine solitons have been derived several decades ago [3, 5–8]. First studied in the context of modulation instability, SFBs have been the subject of a renewed interest in the 2000s because these localized solutions are considered as possible prototypes of rogue waves [9–12]. The PS solution is given by

$$\psi_{PS}(t, z) = \left[1 - \frac{4(1 + 2iz)}{1 + 4t^2 + 4z^2}\right]e^{iz}, \tag{2}$$

and it exhibits the remarkable property to be localized both in space and in time [3]. It has been experimentally generated by using specifically designed initial conditions in optical fibers [13], plasmas [14], and water tank [15].

In a completely different context, pulse compression has been widely studied in the last 4 decades both experimentaly in optical fiber experiments and theoretically by using numerical simulations of the NLSE [2, 16–19]. The goal of these studies was to provide the shortest possible pulse with the highest peak power at the output of the fiber. It is very important to note that these studies have been focused on the so-called higher-order solitons, also named "N-solitons" which means that the initial pulse is "made" of several solitons in the framework of the inverse scattering transform (IST) [20]. As a consequence, it is often considered that the pulse compression arises from the propagation of bound-state multi-soliton solutions [17].

Mathematics has provided in the 2010s a different perspective on pulse compression in focusing regime of the NLSE [1]. It has been rigorously demonstrated that in the semiclassical (zero dispersion) limit of the NLSE, a sufficiently smooth pulse undergoes a gradient catastrophe, that is, the divergence of the derivatives of the field that is regularized by the generation of a coherent structure locally (asymptotically) described by the PS solution.

Very importantly, this theorem provides a local interpretation of the mechanism underlying the pulse compression and links this phenomenon with the famous PS. Note that the result is somehow surprising because the pulse compression is obviously achieved with zero boundary conditions, while the PS is a solution of the NLSE with nonzero boundary conditions. Moreover, this mechanism is universal because it is independent of the soliton content and of the exact shape of the initial pulse. As a consequence, while the exact PS is often seen as the interaction between a plane wave and a soliton [21], the local emergence of the PS arising in the pulse compression does not require the existence of the soliton.

This short review aims at presenting the main mathematical and experimental results related to the local emergence of the PS in the process of pulse compression. We also show the important consequences of this phenomenon on the statistical properties of nonlinear random waves in focusing NLSE systems [22–24].

2 MATHEMATICAL RESULTS: REGULARIZATION OF THE GRADIENT CATASTROPHE IN THE SEMICLASSICAL FOCUSING NLSE

Semiclassical limit is a powerful tool to study large space–time, z, t, behavior of the NLSE (1). It is achieved by introducing a small parameter $0 < \varepsilon \ll 1$ and rescaling $\xi = \varepsilon z, \tau = \varepsilon t, \psi(z, t) \to \psi(\xi, \tau; \varepsilon)$ so that focusing NLSE (1) assumes the form

$$i\varepsilon\psi_\xi + \frac{1}{2}\varepsilon^2\psi_{\tau\tau} + |\psi|^2\psi = 0. \tag{3}$$

In the following, we assume that the amplitude of ψ at $\xi = 0$ is $\mathcal{O}(1)$.

Physically, the nondimensional dispersion parameter ε is determined by the ratio of the nonlinear medium's internal coherence length (the soliton width/duration) and the typical scale of initial data. Therefore, the study of small-dispersion dynamics in (3) is equivalent to the study of the evolution of large-scale data in the original NLSE (1). Importantly, the limit as $\varepsilon \to 0$ in **Eq. 3** enables analysis of solutions to (1) for both large and $\mathcal{O}(1)$ t, z-scales using the same equation.

It is convenient to introduce a Wentzel–Kramers–Brillouin (WKB)-type representation for $\psi(\tau, \xi)$ (the Madelung transform):

$$\psi = \sqrt{\rho}\, e^{i\frac{\phi}{\varepsilon}}, \qquad \phi_\tau = u \tag{4}$$

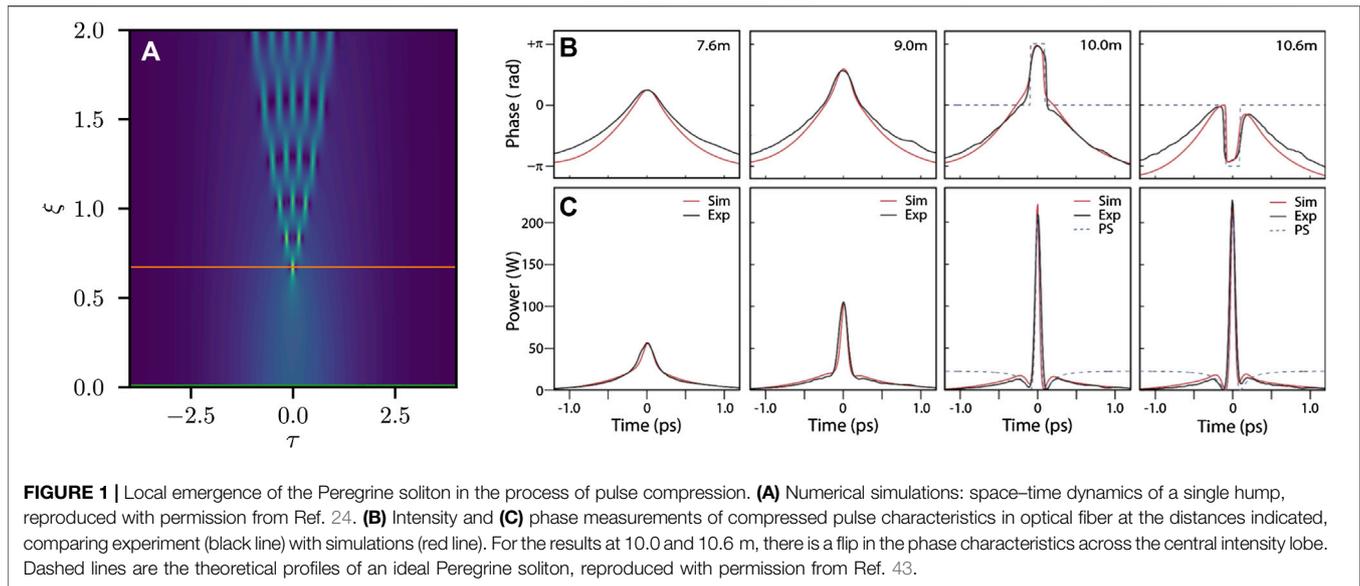to convert the semiclassical NLSE (3) into a system:

$$
\begin{aligned}
&\rho_\xi + (\rho u)_\tau = 0, \\
&u_\xi + uu_\tau - \rho_\tau - \varepsilon^2\left(\frac{\rho_{\tau\tau}}{4\rho} - \frac{\rho_\tau^2}{8\rho^2}\right)_\tau = 0,
\end{aligned}
\tag{5}
$$

for the wave field intensity (power) $\rho(\tau, \xi) = |\psi|^2$ and the "chirp" $u(\tau, \xi)$. Note that the system (5) is strictly equivalent to the NLSE.

The *dispersionless limit* is obtained from (5) by setting $\varepsilon = 0$. In this limit, the system (5) is of elliptic type so that its solutions, when exist, have finite life span due to the development of infinite τ- and ξ-derivatives of ρ and u at some critical point $\tau = \tau_c, \xi = \xi_c$, which is often referred to as a point of gradient catastrophe [25]. In the vicinity of the gradient catastrophe point, the contribution of the dispersive term $\mathcal{O}(\varepsilon^2)$ in (5) becomes significant so that at $\xi > \xi_c$, the emerging regularized dynamics exhibit large-amplitude, ε-scaled oscillations of the intensity signifying the singular nature of the semiclassical $\varepsilon \to 0$ limit. The results reported in this review have been obtained mathematically and realized experimentally for small but nonzero values of ε [1]. Below, we summarize the history of the mathematical ideas underlying these results.

The semiclassical limit of the NLSE is most efficiently studied in the framework of the IST method [20]. At the heart of this theory is a linear differential [Zakharov–Shabat (ZS)] operator whose spectrum is determined by the NLSE wave field $\psi(\tau, \xi)$ playing the role of the scattering potential. Generally, the IST spectrum has two components: discrete and continuous. The discrete component is related to a soliton "content" of $\psi(\tau, \xi)$, while the continuous component corresponds to dispersive wave radiation as $\xi \to \infty$. The potentials $\psi(\tau, \xi)$ having pure continuous spectrum are called solitonless. The IST spectrum is invariant with respect to the NLSE evolution and so can be evaluated at $\xi = 0$.

The study of the semiclassical limit of integrable equations was initiated by Lax and Levermore [26] in the framework of the Korteweg–de Vries (KdV) equation for which the associated scattering operator is self-adjoint. The attempts to extend the Lax–Levermore theory to the focusing NLSE ran into complications due to non–self-adjoint nature of the ZS operator for (3). The first numerical studies [27–29] revealed an τ, ξ-region of the initial evolution of smooth modulated plane wave followed by the emergence of a region filled with rapid nonlinear oscillations exhibiting complex spatiotemporal behavior (see **Figure 1A**). The development of the steepest descent method of Deift–Zhou for matrix Riemann–Hilbert

FIGURE 1 | Local emergence of the Peregrine soliton in the process of pulse compression. **(A)** Numerical simulations: space–time dynamics of a single hump, reproduced with permission from Ref. 24. **(B)** Intensity and **(C)** phase measurements of compressed pulse characteristics in optical fiber at the distances indicated, comparing experiment (black line) with simulations (red line). For the results at 10.0 and 10.6 m, there is a flip in the phase characteristics across the central intensity lobe. Dashed lines are the theoretical profiles of an ideal Peregrine soliton, reproduced with permission from Ref. 43.

problems (RHPs) (see, e.g., [30]) in 1990s led to rigorous mathematical studies of the semiclassical NLSE limit in Ref. 31 (pure discrete spectrum, i.e., solitons only) and in Ref. 32 (both purely radiative (solitonless) cases and radiation with solitons) revealed the detailed micro- and macroscopic structures of the emerging oscillations. In particular, in Ref. 32, the NLSE (**Eq. 3**) evolution of a one-parameter family of modulated plane wave potentials

$$\psi(\tau, 0; \varepsilon) = \operatorname{sech}(\tau) e^{i\phi/\varepsilon}, \quad \phi = -\mu \log(\cosh(\tau)), \qquad (6)$$

where $\mu \in \mathbb{R}$ is the chirp parameter controlling the phase, was studied. The advantage of this family of potentials is that the corresponding scattering data (the IST spectrum) can been calculated explicitly [33]; moreover, its soliton "content" is controlled by the chirp parameter μ; the discrete spectrum component (solitons) is only present when $|\mu| < 2$; otherwise, the spectrum is purely continuous (radiation). The spectrum is purely discrete if and only if $\mu = 0$ and $\varepsilon = \frac{1}{N}$, where $N = 1, 2, \ldots$. In this case, the potential (**6**) represents an exact N-soliton solution of the NLSE (**3**).

The RHP approach allowed establishing rigorous semiclassical asymptotics describing the complex nonlinear dynamics of the NLSE (**3**) with analytic initial data decaying as $|\tau| \to \infty$. In particular, it was shown in Ref. 32 that for the potential (**Eq. 6**), the initial evolution is approximated at leading order in ε by the solution of the dispersionless NLSE ($\varepsilon = 0$ in (**Eq. 5**)) that undergoes gradient catastrophe at the point $(\tau_c, \xi_c) = (0, \frac{1}{\mu+2})$ (see Ref. 34 for broader class of initial data $\psi(\tau, 0; \varepsilon)$).

It was shown in Ref. 1 that if the gradient catastrophe occurs (for $\varepsilon = 0$), it exhibits a regularization mechanism (for $\varepsilon \neq 0$) *via* the emergence of a localized coherent structure, which is asymptotically close to PS (**2**). The mechanism is universal because it does not depend on the particular form of initial data $\psi(\tau, 0; \varepsilon)$. Specifically, it was shown that the solution at the point of maximum localization $\tau_m = \tau_c + \mathcal{O}(\varepsilon^{4/5})$, $\xi_m = \xi_c + \mathcal{O}(\varepsilon^{4/5})$ assumes the form $|\psi(\tau, \xi_m)| =$

$a_0 [1 - 4/(1 + 4a_0^2((\tau - \tau_m)/\varepsilon)^2)](1 + \mathcal{O}(\varepsilon^{1/5}))$, where $a_0 = \sqrt{\rho(0, \xi_c)} + \mathcal{O}(\varepsilon^{1/5})$ is the background amplitude, that is, it is determined at the leading order by the value of instantaneous power at the gradient catastrophe point. In the case of potential (**6**), it was found that $\rho(0, \xi_c) = \mu + 2$. The maximum value of $|\psi|$ in the local PS is then $3a_0$ and is determined up to $\mathcal{O}(\varepsilon^{1/5})$. We stress that the above approximate PS solution is valid locally, in the ε-vicinity of the point (τ_m, ξ_m).

Importantly, the effect of the local emergence of the PS right beyond the gradient catastrophe point is universal and does not depend on the composition of the (global) IST spectrum of the initial data. In other words, the initial condition for (**5**) can have high soliton content or be completely solitonless—in all cases, the PS appears as a nonlinear coherent structure locally regularizing the gradient catastrophe. The specific form of the initial condition affects only the time ξ_m of the PS development.

3 LOCAL EMERGENCE OF THE PEREGRINE SOLITON IN EXPERIMENTS WITH SINGLE PULSE

The self-compression of pulses has been a very widely investigated topic experimentally, especially since the first observation of solitonic behavior in optical fibers in 1980 [35]. Indeed, it has been observed that the propagation of solitonic pulses with sufficiently high initial peak power is always accompanied, at first, by a narrowing of the pulses and an increase in their peak power before eventually undergoing successive splittings. These observations have been successfully compared to the well-known dynamics of higher-order solitons or "N-solitons" such that the phenomenon of pulse self-compression was referred to as the "Soliton effect" [2, 36, 37]. This effect has been widely studied [16, 38], including the two-stage compression technique [39] and higher-order effects [40, 41].

In the context of 1-D hydrodynamics experiments, similar dynamics have been observed in the compression of the envelope of $N = 2$ and $N = 3$ solitons, which suggests that the underlying mechanism may be of the same origin [42].

The recent mathematical results described above provide a new interpretation of the mechanism underlying most of the past experiments on what was called "soliton self-compression." Two main ideas are important: (i) the mechanism actually does not depend on the soliton content of the pulse and (ii) the Peregrine soliton emerges locally as the regularization of gradient catastrophe.

Point (ii) has been recently demonstrated in optical fiber experiments [43] using two different setups. In particular, picosecond pulses with a peak power $P_0 = 26.3$ W have been injected into a Ge-doped highly nonlinear optical fiber. The input pulses were well fitted by a sech profile corresponding to a soliton of an order $N \approx 6$, that is, $\varepsilon \approx 0.16$. These experiments were performed for different fiber lengths, and a complete characterization of the compressed pulse in both amplitude and phase was achieved using the FROG technique [44]. The retrieved intensity (bottom) and phase (top) at the fiber lengths indicated, comparing experiment (black line) with simulations (red line), are plotted in **Figures 1B,C**. In all cases, there is an excellent agreement between experiment and simulation. Importantly, the intensity and phase profiles of an ideal PS solution match very well the experiment and simulation across the pulse center while approaching the maximum compression point (for the lengths of the fiber around 10 m). The main difference is that the PS solution is characterized by the background that extends to $\tau \to \pm\infty$, whereas the pedestal observed in experiments is limited by the temporal width of the input pulse. As explained above, the emergence of the PS here is a local dynamical mechanism. As observed in **Figure 1B**, the π phase jump occurring at zero intensity between the central lobe and the background pedestal is a remarkable signature of the PS. Moreover, the change of the sign of the phase derivative across the maximum compression point, another characteristic of the exact PS solution, is also observed in the experiments between 10 and 10.6 m.

It is important to note that the experimental results of [43] show that the mechanism demonstrated in the semiclassical limit of NLSE [1] is very robust and can be observed over a very broad range of ε. The PS is observed at the maximum compression point of the pulse as long as $\varepsilon = \sqrt{L_D/L_{NL}} \leq 0.5$ $(N > 2)$.

4 STATISTICAL SIGNATURES IN NONLINEAR RANDOM WAVE EVOLUTION

Recent studies have shown that the dynamical mechanism leading to the local emergence of the PS (see **Sections 3** and **4**) plays a crucial role in the emergence of rogue waves (RWs) and in the statistics of integrable turbulence [22–24]. *Integrable turbulence* corresponds to complex dynamical phenomena arising along the nonlinear propagation of random waves in a system governed by an integrable equation such as the NLSE [22, 43, 45–49].

An important example of integrable turbulence in NLSE systems arises when the initial field corresponds to the linear superposition of numerous *independent* Fourier components:
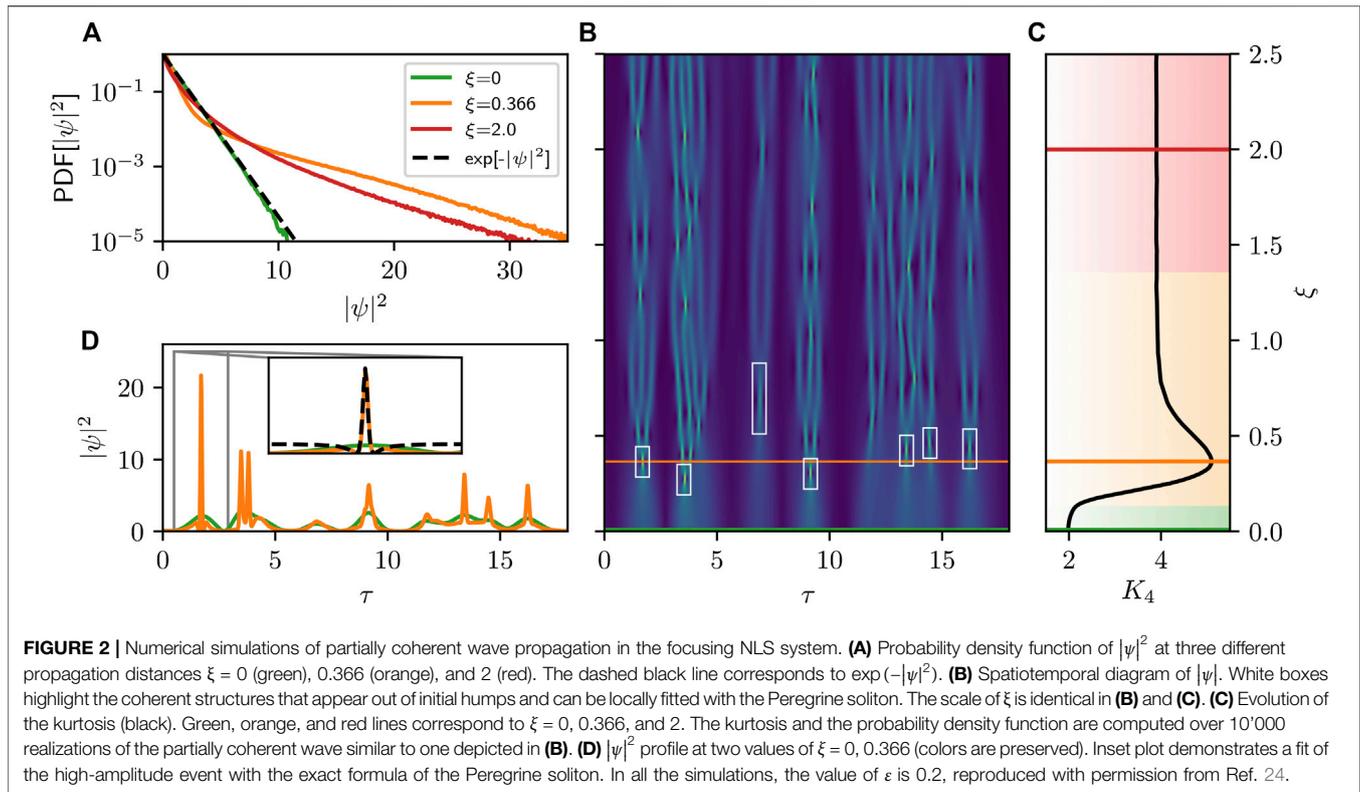
$$\psi(\tau, \xi) = \sum_k a_k(\xi) e^{\frac{2\pi i}{T} k\tau} \text{ with } k \in \mathbb{Z}. \tag{7}$$

Here, periodic boundary conditions with a period T are used, and $a_k(0) = |a_{0k}| e^{i\phi_{0k}}$ is a kth Fourier component with a uniformly distributed random phase $\phi_{0k} \in [-\pi, \pi]$. This kind of partially coherent waves is fundamental because of the omnipresence, in natural environments, of stochastic waves with a finite Fourier spectrum having delta-correlated frequency components. The central limit theorem shows that the statistics of ψ given by **Eq. 7** is Gaussian and the statistics of $|\psi|^2$ is exponential [46].

First observed in the open sea, RWs have been studied in a large variety of nonlinear media and can be defined as extreme (high-amplitude) events that appear more frequently than predicted by the linear theory [11]. Experimental investigations of the evolution of the partially coherent wave first in a water tank [50] and later in controlled optical fiber experiments well described by the NLSE [46] demonstrated the emergence of non-Gaussian statistics. An example of corresponding numerical simulation is shown in **Figure 2**, where the nonlinear propagation of partially coherent initial condition characterized by the exponential distribution for $|\psi|^2$ (depicted by green in plots in **Figures 2A,D**) leads to the heavy-tailed probability density function (**Figure 2A** orange and red lines)—the main evidence of the rogue wave emergence.

It is important to note that at present, there is no theory describing these statistical properties in the focusing 1-D NLSE system [22, 23, 46, 49]. However, remarkably, the local PSs (see, e.g., inset in **Figure 2D**), previously considered as a prototype of RWs, were identified in numerical simulations of the NLSE, reported along with the pioneering experimental observations. By using temporal imaging techniques, it has been proved that the temporal *intensity* profile of some extreme events emerging during the evolution of partially coherent light in optical fibers resembles the localized PS [22]. Recent advances of heterodyne time microscopy have enabled the ultrafast single-shot measurement of both phase and amplitude of random waves [23]. By using this technique, the local emergence of the PS embedded in partially coherent waves propagating in optical fibers has been fully demonstrated [23]. Having access to the phase and intensity profiles, it becomes possible to reconstruct the complex amplitude and, therefore, numerically find the initial structure resulting in the RW simply by simulating the reversed NLSE. Such nonlinear temporal holography revealed that the typical structure that leads to the RW emergence is a large initial hump. This observation constitutes the first solid evidence of the gradient catastrophe regularization playing a role in the nonlinear dynamics of partially coherent waves. Note that similar observations have been made in deep water wave experiments [51, 52].

A systematic study of the local PS emergence in integrable turbulence behind the 1-D NLSE has been provided first numerically [24] and later verified experimentally in a 1-D water tank [52]. Employing the robust theoretical results

FIGURE 2 | Numerical simulations of partially coherent wave propagation in the focusing NLS system. **(A)** Probability density function of $|\psi|^2$ at three different propagation distances $\xi = 0$ (green), 0.366 (orange), and 2 (red). The dashed black line corresponds to $\exp(-|\psi|^2)$. **(B)** Spatiotemporal diagram of $|\psi|$. White boxes highlight the coherent structures that appear out of initial humps and can be locally fitted with the Peregrine soliton. The scale of ξ is identical in **(B)** and **(C)**. **(C)** Evolution of the kurtosis (black). Green, orange, and red lines correspond to $\xi = 0$, 0.366, and 2. The kurtosis and the probability density function are computed over 10'000 realizations of the partially coherent wave similar to one depicted in **(B)**. **(D)** $|\psi|^2$ profile at two values of $\xi = 0$, 0.366 (colors are preserved). Inset plot demonstrates a fit of the high-amplitude event with the exact formula of the Peregrine soliton. In all the simulations, the value of ε is 0.2, reproduced with permission from Ref. 24.

described in **Section 2**, a strong correlation between the distribution of lengths of local PS maximum compression and the most probable distances of the RW emergence has been found. Assuming that local humps present in the initial conditions evolve independently at least before the gradient catastrophe point, maximum compression points were estimated for each of them locally by renormalizing the NLSE according to the hump's amplitude and duration. The computed probability density of the local PS emergence position took a shape of an asymmetric overshoot having a distinct maximum. As a measure of deviation from the Gaussian distribution, and therefore, the increased probability of RW observation, a fourth moment of the distribution (kurtosis) was employed. The presence of the overshoot in the kurtosis evolution for partially coherent initial conditions (see **Figure 2C**) has been shown in Ref. 53. Numerical simulations reported in Ref. 24 demonstrate a remarkable correlation between these two overshoots, implying that the area of the highest probability of observation of the extreme events in the evolution of partially coherent waves in the focusing 1-D NLS model is directly related to the local emergence of PSs as a regularization of the gradient catastrophe. As well as for the deterministic initial conditions described in **Section 3**, this effect remains valid beyond the formal applicability of the results reported in Ref. 1.

5 DISCUSSION

The PS has been originally discovered as a breather solution of the focusing NLSE (with nonzero boundary conditions) that exhibits

the remarkable property to be localized both in space and time [3]. It has been observed in experiments made in the 2000s with plasma waves [14], water waves [15], and optical waves [13]. In the 2010s, it has been shown mathematically that the PS also emerges locally as a universal mechanism of dispersive regularization of a gradient catastrophe arising in the self-focusing evolution of an initially broad pulse [1]. This mechanism of local emergence of the PS is universal in the sense that it depends neither on the exact shape of the initial pulse nor on its soliton content. The understanding that the PS emerges locally in the process of self-focusing of a broad wave packet [43] has shed new light on the self-compression of light pulses, which has been extensively studied in the fiber optics community in the 1980s.

The dynamical process of the emergence of the PS in the evolution of broad and smooth wave packets is highly relevant in the context of integrable turbulence where the nonlinear evolution of partially coherent waves is investigated at the statistical level. Partially coherent waves with an initial Gaussian statistics are indeed composed of a random collection of large humps (see **Figure 2**) which individually experience the self-focusing process leading to the gradient catastrophe regularized by the emergence of the PS [24]. As shown in Ref. [24], this feature explains well the behavior followed by statistical moments of the wave field such as the kurtosis. Remarkably, a similar conclusion draws from the large deviation theory with applications to the stochastic water wave dynamics [54].

The scenario of the local emergence of the PS in the regularization of a gradient catastrophe is expected to be robust against some perturbations such as dissipation and forcing [55, 56], and higher-order nonlinear effects [57].

However, the investigation of the role of higher-order effects now represents essentially an open question.

AUTHOR CONTRIBUTIONS

All the authors wrote this mini review. ATo is the author of the key mathematical results reported in **Section 2**. PS, GE, SR, and ATi are authors of experimental and numerical results reported in **Sections 3** and **4**.

REFERENCES

1. Bertola M, Tovbis A. Universality for the focusing nonlinear Schrödinger equation at the gradient catastrophe point: rational breathers and Poles of the Tritronquée Solution to Painlevé I. *Commun Pure Appl Math* (2013) 66: 678–752. doi:10.1002/cpa.21445

2. Mollenauer LF, Tomlinson WJ, Stolen RH, Gordon JP. Extreme picosecond pulse narrowing by means of soliton effect in single-mode optical fibers. *Opt Lett* (1983) 8:289–91. doi:10.1364/OL.8.000289

3. Peregrine DH. Water waves, nonlinear Schrödinger equations and their solutions. *J Aust Math Soc Ser B Appl Math* (1983) 25:16–43. doi:10.1017/S0334270000003891

4. Akhmediev NN, Ankiewicz A. *Solitons: nonlinear pulses and beams*. London: Chapman & Hall (1977).

5. Kuznetsov EA. Solitons in a parametrically unstable plasma. *DoSSR* (1977) 236: 575–7

6. Kawata T, Inoue H. Inverse scattering method for the nonlinear evolution equations under nonvanishing conditions. *J Phys Soc Jpn* (1978) 44:1722–9. doi:10.1143/jpsj.44.1722

7. Ma Y-C. The perturbed plane-wave Solutions of the cubic Schrödinger equation. *Stud Appl Math* (1979) 60:43–58. doi:10.1002/sapm197960143

8. Akhmediev NN, Eleonskii VM, Kulagin NE. Exact first-order solutions of the nonlinear Schrödinger equation. *Theor Math Phys* (1987) 72:809–18. doi:10.1007/bf01017105

9. Dysthe KB, Trulsen K. Note on breather type solutions of the nls as models for freak-waves. *Phys Scripta* (1999) T82:48. doi:10.1238/physica.topical.082a00048

10. Akhmediev N, Ankiewicz A, Taki M. Waves that appear from nowhere and disappear without a trace. *Phys Lett* (2009) 373:675–8. doi:10.1016/j.physleta.2008.12.036

11. Onorato M, Residori S, Bortolozzo U, Montina A, Arecchi FT. Rogue waves and their generating mechanisms in different physical contexts. *Phys Rep* (2013) 528:47–89. doi:10.1016/j.physrep.2013.03.001

12. Dudley JM, Dias F, Erkintalo M, Genty G. Instabilities, breathers and rogue waves in optics. *Nat Photon* (2014) 8:755–64. doi:10.1038/nphoton.2014.220

13. Kibler B, Fatome J, Finot C, Millot G, Dias F, Genty G, et al. The Peregrine soliton in nonlinear fibre optics. *Nat Phys* (2010) 6:790–5. doi:10.1038/nphys1740

14. Bailung H, Sharma SK, Nakamura Y. Observation of peregrine solitons in a multicomponent plasma with negative ions. *Phys Rev Lett* (2011) 107:255005: doi:10.1103/PhysRevLett.107.255005

15. Chabchoub A. Tracking breather dynamics in irregular sea state conditions. *Phys Rev Lett* (2016) 117:144103. doi:10.1103/PhysRevLett.117.144103

16. Dianov EM, Nikonova ZS, Prokhorov AM, Serkin VN. Optimal compression of multi-soliton pulses in optical fibers. *Sov Tech Phys Lett* (1986) 12:311–3

17. Akhmediev N, Betina L, Eleonskiĭ V, Kulagin N, Ostrovskaya NV, Poltoratskiĭ ÉA. Optimal self-compression of multisoliton pulses in an optical fiber. *Sov J Quant Electron* (1989) 19:1240. doi:10.1070/qe1989v019n09abeh009130

18. JR Taylor ed. *Optical solitons theory and experiment*. Cambridge: Cambridge University Press (1992).

19. Agrawal GP. *Nonlinear fiber optics*. London: Academic Press (2013).

20. Zakharov V, Shabat AB. Exact theory of two-dimensional self-focusing and one-dimensional self-modulation of waves in non linear media. *Sov Phys JETP* (1972) 34:62–9

21. Biondini G, Kovačič G. Inverse scattering transform for the focusing nonlinear schrödinger equation with nonzero boundary conditions. *J Math Phys* (2014) 55:031506. doi:10.1063/1.4868483

22. Suret P, El Koussaifi R, Tikan A, Evain C, Randoux S, Szwaj C, et al. Single-shot observation of optical rogue waves in integrable turbulence using time microscopy. *Nat Commun* (2016) 7:13136. doi:10.1038/ncomms13136

23. Tikan A, Bielawski S, Szwaj C, Randoux S, Suret P. Single-shot measurement of phase and amplitude by using a heterodyne time-lens system and ultrafast digital time-holography. *Nat Photon* (2018) 12:228–34. doi:10.1038/s41566-018-0113-8

24. Tikan A. Effect of local peregrine soliton emergence on statistics of random waves in the one-dimensional focusing nonlinear schrödinger equation. *Phys Rev E* (2020) 101:012209. doi:10.1103/physreve.101.012209

25. Dubrovin B, Grava T, Klein C. On Universality of critical behavior in the focusing nonlinear Schrödinger equation, elliptic Umbilic catastrophe and the Tritronquée Solution to the Painlevé-I equation. *J Nonlinear Sci* (2009) 19: 57–94. doi:10.1007/s00332-008-9025-y

26. Lax PD, David Levermore C. The small dispersion limit of the Korteweg–de Vries equation. I. *Commun Pure Appl Math* (1983) 36, 253–90. doi:10.1002/cpa.3160360302

27. Bronski JC. Semiclassical eigenvalue distribution of the Zakharov–Shabat eigenvalue problem. *Phys Nonlinear Phenom* (1996) 97, 376–97. doi:10.1016/0167-2789(95)00311-8

28. Bronski JC, Nathan Kutz J. Numerical simulation of the semi-classical limit of the focusing nonlinear Schrödinger equation. *Phys Lett* (1999) 254:325–36. doi:10.1016/s0375-9601(99)00133-4

29. Cai D, McLaughlin DW, McLaughlin KT. The nonlinear schrödinger equation as both a pde and a dynamical system. In *Handbook of dynamical systems. vol. 2* Amsterdam: Elsevier (2002). p. 599–675.

30. Deift P, Venakides S, Zhou X. New results in small dispersion KdV by an extension of the steepest descent method for Riemann-Hilbert problems. *Int Math Res Not* (1997) 1997:286–99. doi:10.1155/S1073792897000214

31. Kamvissis S, McLaughlin KDT-R, Miller PD. Semiclassical soliton ensembles for the focusing nonlinear Schrödinger equation. Princeton: Princeton University Press (2003).

32. Tovbis A, Venakides S, Zhou X. On semiclassical (zero dispersion limit) solutions of the focusing nonlinear Schrödinger equation. *Commun Pure Appl Math* (2004) 57:877–985. doi:10.1002/cpa.20024

33. Tovbis A, Venakides S. The eigenvalue problem for the focusing nonlinear Schrödinger equation: new solvable cases. *Physica D: Nonlinear Phenomena* (2000) 146:150–64. doi:10.1016/S0167-2789(00)00126-3

34. Tovbis A, Venakides S, Zhou X. Semiclassical focusing nonlinear Schrodinger Equation I: inverse scattering map and its evolution for radiative initial data. *Int Math Res Not* (2007) 20:12–9. doi:10.1093/imrn/rnm094

35. Mollenauer LF, Stolen RH, Gordon JP. Experimental observation of picosecond pulse narrowing and Solitons in optical fibers. *Phys Rev Lett* (1980) 45:1095–8. doi:10.1103/PhysRevLett.45.1095

36. Mitschke FM Mollenauer LF. Ultrashort pulses from the soliton laser. *Opt Lett* (1987) 12:407. doi:10.1364/OL.12.000407

37. Potasek MJ. Experimental and numerical results of optical subpulse formation of long optical pulses in monomode fibers. *Opt Lett* (1987) 12:717. doi:10.1364/OL.12.000717

38. Agrawal GP. *Applications of nonlinear fiber optics*. London: Academic Press (2001).

39. Tai K, Tomita A. 1100× optical fiber pulse compression using grating pair and soliton effect at 1.319 μm. *Appl Phys Lett* (1986) 48:1033–5. doi:10.1063/1.96639

40. Beaud P, Hodel W, Zysset B, Weber H. Ultrashort pulse propagation, pulse breakup, and fundamental soliton formation in a single-mode optical fiber. *IEEE J Quant Electron* (1987) 23:1938–46. doi:10.1109/JQE.1987.1073262

41. Gouveia-Neto AS, Gomes ASL, Taylor JR. Generation of 33-fsec pulses at 132 μm through a high-order soliton effect in a single-mode optical fiber. *Opt Lett* (1987) 12:395. doi:10.1364/OL.12.000395

42. Chabchoub A, Hoffmann N, Onorato M, Genty G, Dudley JM, Akhmediev N. Hydrodynamic supercontinuum. *Phys Rev Lett* (2013b) 111:054104. doi:10.1103/PhysRevLett.111.054104

43. Tikan A, Billet C, El G, Tovbis A, Bertola M, Sylvestre T, et al. Universality of the peregrine soliton in the focusing dynamics of the cubic nonlinear schrödinger equation. *Phys Rev Lett* (2017) 119:033901. doi:10.1103/physrevlett.119.033901

44. Trebino R. *Frequency-resolved optical Gating: the measurement of ultrashort laser pulses*. Berlin: Springer (2002).

45. Zakharov VE (2009). Turbulence in integrable systems. *Stud Appl* 122:219–34. doi:10.1111/j.1467-9590.2009.00430.x

46. Walczak P, Randoux S, Suret P. Optical rogue waves in integrable turbulence. *Phys Rev Lett* (2015) 114:143903. doi:10.1103/PhysRevLett.114.143903

47. Agafontsev DS, Zakharov VE. Integrable turbulence and formation of rogue waves. *Nonlinearity* (2015) 28:2791. doi:10.1088/0951-7715/28/8/2791

48. Soto-Crespo JM, Devine N, Akhmediev N. Integrable turbulence and rogue waves: breathers or solitons? *Phys Rev Lett* (2016) 116:103901. doi:10.1103/PhysRevLett.116.103901

49. Copie F, Randoux S, Suret P. The physics of the one-dimensional nonlinear schrödinger equation in fiber optics: rogue waves, modulation instability and self-focusing phenomena. *Rev Phys* (2020) 14:10–37. doi:10.1016/j.revip.2019.100037

50. Onorato M, Osborne AR, Serio M, Cavaleri L, Brandini C, Stansberg CT. Observation of strongly non-Gaussian statistics for random sea surface gravity waves in wave flume experiments. *Phys Rev E* (2004) 70:067302. doi:10.1103/PhysRevE.70.067302

51. Cazaubiel A, Michel G, Lepot S, Semin B, Aumaître S, Berhanu M, et al. Coexistence of solitons and extreme events in deep water surface waves. *Phys Rev Fluids* (2018) 3:114802. doi:10.1103/PhysRevFluids.3.114802

52. Michel G, Bonnefoy F, Ducrozet G, Prabhudesai G, Cazaubiel A, Copie F, et al. Emergence of peregrine solitons in integrable turbulence of deep water gravity waves. *Phys Rev Fluids* (2020) 5:082801. doi:10.1103/PhysRevFluids.5.082801

53. Onorato M, Proment D, El, G, Randoux S, Suret P. On the origin of heavy-tail statistics in equations of the Nonlinear Schrödinger type. *Phys Lett* (2016) 380:3173–7. doi:10.1016/j.physleta.2016.07.048

54. Dematteis G, Grafke T, Onorato M, Vanden-Eijnden E. Experimental evidence of hydrodynamic instantons: the universal route to rogue waves. *Phys Rev X* (2019) 9:041057. doi:10.1103/PhysRevX.9.041057

55. Fotopoulos G, Frantzeskakis DJ, Karachalios NI, Kevrekidis PG, Koukouloyannis V, Vetas K. Extreme wave events for a nonlinear Schrödinger equation with linear damping and Gaussian driving. *Commun Nonlinear Sci Numer Simulat* (2020) 82:105058. doi:10.1016/j.cnsns.2019.105058

56. Chabchoub A, Hoffmann N, Branger H, Kharif C, Akhmediev N. Experiments on wind-perturbed rogue wave hydrodynamics using the peregrine breather model. *Phys Fluids* (2013a) 25:101704. doi:10.1063/1.4824706

57. Dudley JM, Genty G, Coen S. Supercontinuum generation in photonic crystal fiber. *Rev Mod Phys* (2006) 78:1135–84. doi:10.1103/RevModPhys.78.1135